DEEPIKA KOUNDAL[1A], SAVITA GUPTA[2B], SUKHWINDER SINGH[2C]

[a]koundal@gmail.com, [b]savita2k8@yahoo.com, [c]sukhdalip@yahoo.com
[1]Chitkara University, Rajpura, Punjab
[2]University Institute of Engineering & Technology, Panjab University, Chandigarh, India

Applications of Neutrosophic Sets in Medical Image Denoising and Segmentation

Abstract

In medical science, diagnosis and prognosis is one of the most difficult and challenging task because of restricted subjectivity of the experts and presence of fuzziness in medical images. In observing the severity of several diseases, different professional experts may result in wrong diagnosis. In order to perform diagnosis intuitively in the medical images, different image processing methods have been explored in terms of neutrosophic theory to interpret the inherent uncertainty, ambiguity and vagueness. This paper demonstrates the use of neutrosophic theory in medical image denoising and segmentation where the performance is observed to be much better.

Keywords

Neutrosophic logic, fuzzy logic, image segmentation.

1. Introduction

Generally medical images are consisted of fuzziness and imprecision information, therefore segmentation, feature extraction and classification are difficult to perform [1]. Since fuzzy sets are widely used for processing fuzziness and uncertainty in a wide range of fields such as control science and image processing [2]. But the limitation of this method is that it does not consider the spatial context of the pixels due to noise and artifacts [3]. The generalization of fuzzy set in form of neutrosophic set is becoming more popular in image processing tasks to overcome the limitations of fuzzy based approaches. The concept of Neutrosophy is introduced by Smarandache [4]. Neutrosophy is the foundation of neutrosophic probability, neutrosophic statistics, neutrosophic logic and neutrosophic set [4]. *Neutrosophic set* generalizes the concept of the classic set, fuzzy set, interval valued fuzzy set [5], intuitionistic fuzzy set [6], paraconsistent set, paradoxist set, tautological set, dialetheist set [3]. *Neutrosophy theory* takes into account every theory, concept, or entity <*A*> in relation to its opposite, <*Anti-A*> and <*Non-A*>. The neutralities <Neut-A> which is not *A,* and that which is neither <*A*> nor <*Anti-A*> are referred to as <*Non-A*>. In *neutrosophic logic*, three neutrosophic components: *T, I, F* are defined to estimate the truth

membership degree, the false membership degree, and the indeterminacy membership degree (neither true nor false) in <*A*>. Unlike fuzzy logic, neutrosophic logic introduces the extra domain *I* which provides a more efficient way to handle higher degrees of uncertainty that is very difficult for fuzzy logic to be handled [7]. The major difference between a Neutrosophic Set (NS) and a Fuzzy Set (FS) is that there is no limit on the sum *m* in a NS, while in a FS *m (m=t+f)* must be equal to 1 [8]. The Neutrosophic image domain is shown in Fig. 1.

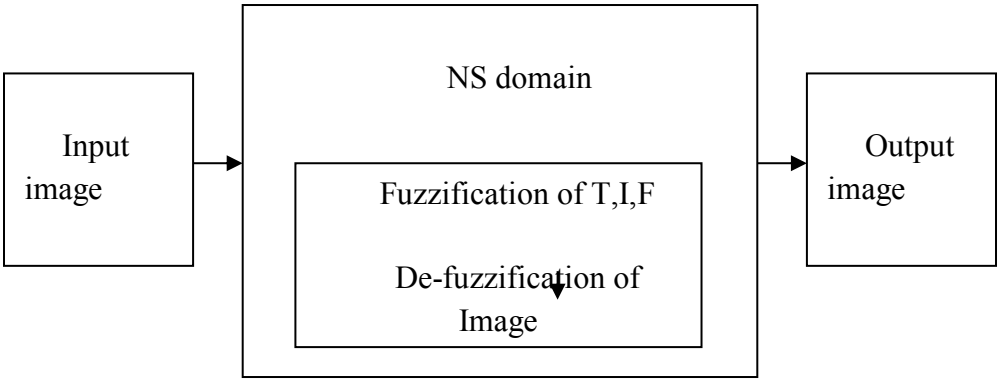

Figure 1. *Neutrosophic Image Domain*

A neutrosophic image is characterized by three subsets *T, I* and *F*. A pixel P in neutrosophic image is described as *P(i ,j), { T(i ,j), I(i ,j), F(i ,j)}*. Thus, for each pixel in the neutrosophic image, the truth degree *T,* false degree *F* and indeterminacy degree *I* is required to be computed. In general, a NS is symbolized as <*T, I, F*>. In case of determining the tumor in image, tumor can be considered as <*A*>, boundaries as <*Neut-A*> and background as <*Anti-A*>. *T, I,* and *F* are the neutrosophic components to represent <*A*>, <*Neut-A*> and <*Anti-A*>, <*A*> and <*Anti-A*> contain region information, while <*Neut-A*> has boundary information [9, 10].

A pixel in the neutrosophic image can be represented as $A\{t, i, f\}$, where $t\%$ represents true (tumor), $i\%$ represents indeterminate (boundaries) and $f\%$ represents false (background), where $t \in T$, $i \in I$ and $f \in F$ [7]. In the FS, $i = 0, 0 \leq t, f \leq 100$. In the NS, $0 \leq t, i, f \leq 100$ [11,12]. An element $x(t, i, f)$ belongs to the set in the following way: it is t true in the set, i indeterminate in the set, and f false, where $t, i,$ and f are real numbers taken from the sets $T, I,$ and F with no restriction on T, I, F nor on their sum $m = t + i + f$. In literature, number of neutrosophic based denoising and segmentation methods are given [13, 14, 15, 21, 23, 29].

The rest of paper is organized in four sections. Section 2 describes the neutrosophic based image denoising and segmentation methods. Section 3 discusses the results of various neutrosophic domain methods. Finally, the conclusion is summarized in Section 4.

2. Neutrosophic Based Image Processing

1.1. Transformation of Image in Neutrosophic Domain

TM, IM and FM are the neutrosophic components to represent $< A >$, $< Neut - A >$ and $< Anti - A >$ respectively in neutrosophic domain. Every neutrosophic pixel can be represented as

$P_{NI} = \{TM, IM, FM\}$, where TM is the set of white pixels, IM is the set of indeterminate pixels and FM is the set of non-white pixels respectively [16, 17]. The membership functions TM, IM and FM are computed as

$$TM = \frac{\hat{f}_{ij} - \hat{f}_{min}}{\hat{f}_{max}} \tag{1}$$

where i differs from 0 to *n-1, j* differs from 0 to m-*1,* $\hat{f}_{ij}$ is local mean obtained using window, $\hat{f}_{min}$ is minimum intensity value and $\hat{f}_{max}$ is the maximum intensity value.

$$\hat{f}_{ij} = \frac{1}{w \times w} \sum_{m=i-\frac{w}{2}}^{i+\frac{w}{2}} \sum_{n=j-\frac{w}{2}}^{j+\frac{w}{2}} f_{mn} \tag{2}$$

where w is a window size, f_{mn} is the noisy image and $\hat{f}_{ij}$ is local mean of pixels on w.

$$IM = \frac{\delta_{ij} - \delta_{min}}{\delta_{max}} \tag{3}$$

$$\delta_{ij} = abs(f_{ij} - \hat{f}_{ij}) \tag{4}$$

where δ_{ij} is absolute difference value between local mean value $\hat{f}_{ij}$ and intensity f_{ij} , δ_{max} is the maximum absolute difference value and δ_{min} is minimum absolute difference value. The false membership is computed as

$$FM = 1 - TM \tag{5}$$

The true subset, TM, is computed by normalizing the intensity values in $[0,1]$ as given in Eq.(1). In ultrasound images, pixels belonging to speckle and texture are hard to differentiate, hence, $\hat{f}_{ij}$, is calculated to ascertain the neighborhood mean of pixels in a kernel. Absolute difference is used to determine the indeterminate component and False subset, FM , is determined as the complement of TM [18].

2.2. Related Work on Neutrosophic Domain image denoising

Several denoising methods based on neutrosophic set have been proposed in the literature to remove Speckle noise, Gaussian and Rician noise [19-28]. Various notions and theories based on NS are defined and applied for denoising of images. The image is converted into the NS domain and γ-median-filtering operation is used to decrease the image indeterminacy. The experiments have been carried out on natural images with various levels of noise for better image denoising [16].

A wiener filter in neutrosophic domain has been introduced in literature for removal of Rician noise. The wiener filtering operation is employed on true and false subsets for the reduction of the noise and indeterminacy. Experiments have been performed on simulated MRI from Brainweb database and clinical MR images, which are affected by Rician noise [22]. It has been found that wiener filter in neutrosophic domain is able to preserve edges with the suppression of Rician noise.

In [25, 26], LEE and KUAN filter were implemented in neutrosophic domain for the reduction of speckle noise [27]. The Neutrosophic Nonconvex Regularizer Speckle Noise Removal (NNRSNR) method based on Gamma statistics in neutrosophic domain is presented in [28]. Another method based on Nakagami distribution statistics (NTV) which is presented in [29] is further explored in neutrosophic domain. Neutrosophic Nakagami Total Variation method (NNTV) is presented to exploit the Nakagami statistics in neutrosophic domain [30].

2.3. Related work on Neutrosophic Domain Image Segmentation

Recently, neutrosophic based methods have been attracted attention in solving image segmentation problems due to their high performance and indeterminacy handling capability. In literature, several authors have reported number of segmentation methods based on NS [31-40].

Zhang et al. [7] introduced an algorithm, which used the region merge method in NS for the segmentation of natural images to resolve over-segmentation problem. The region merge algorithm started with initial seeds and merged the two regions until a stopping criterion is satisfied. The cluster center is selected on the basis of histogram features in fuzzy domain and the region merge criterion is defined in intensity domain based on edge value and standard deviation features.

Cheng et al. [31] introduced the NS approach with image thresholding for the segmentation of artificial and natural images with indeterminacy handling capability. However, selection of particular threshold value is a critical task as well as it ignores the spatial information and is noise sensitive. Guo et al.[32] presented the fuzzy c-means clustering in NS domain. In this method, entropy in NS domain is used to estimate the indeterminacy of image and α-mean operation is presented to decrease the indeterminacy to make the image more homogenous. Then, image is segmented using a fuzzy c-means clustering. The membership value in the fuzzy clustering is updated as per the indeterminacy value. The experimental analysis demonstrated that the method performed better on both clean and noisy images. Another NS based image segmentation method is presented in which two new operations are defined to reduce the indeterminacy of the image. Zhang et al. [33] presented a watershed segmentation approach in NS domain. In the first phase, image is mapped to NS domain and then, neutrosophic logic and thresholding is used to get a binary image. Final segmentation result is obtained from watershed method. The Neutrosophic Watershed (NW) method has better performance on non-uniform as well as on noisy images.

Further NS is integrated with Improved Fuzzy C-Means (IFCM) for image segmentation [34]. In this, membership degree and convergence criterion of clustering are redefined accordingly. Experimental results demonstrated that the method segmented the images effectively and accurately. Another method named as Neutrosophic C-Means (NCM) clustering is introduced for uncertain data clustering, which is inspired from fuzzy c-means and the NS framework [35]. In this method, the clustering problem is derived as an objective function and is minimized with both

ambiguity rejection and distance rejection. These measures are able to manage uncertainty due to imprecise definition of the clusters.

Another automatic segmentation approach is presented by Sengur et al. [36] which is the combination of texture information with color information in NS and wavelet domain. The method is used for the segmentation of natural color image using γ-K-means clustering. The cluster number K is ascertained with cluster validity analysis. Experiments demonstrated that it segmented the natural images very effectively even if the texture and color of each region does not have homogeneous statistical characteristics. Shan *et al.* [37] presented a clustering method named as Neutrosophic L-Means (NLM) clustering for segmentation of breast ultrasound images. The method achieved the best accuracy with a fairly rapid processing speed. The main limitation of the method is that it is not able to segment multiple-lesions and failed under severe shadowing effect.

Karabatak et al.[38] has given a color image segmentation method in neutrosophic domain. Firstly, the image is transformed into NS domain by defining three membership sets. Then α-mean and β-enhancement operations were used to reduce the indeterminacy. The method suffered from over-segmentation and fixed parameters. An Iterative Neutrosophic Lung Segmentation (INLS) method has been introduced which is based on Expectation-Maximization (EM) analysis and Morphological operations (EMM) for the segmentation of ribs and lungs [39]. The results have shown that the images without or with lung diseases are segmented out more properly.

Guo *et al*. [40] has introduced a method for image based on the NS filter and level set. In First the image is transformed into NS domain by true, false and indeterminacy membership sets. Subsequently, a filter is applied for reduction of noise and level set for image segmentation. Further, a Neutrosophic Edge Detection (NSED) method is presented for edges detection with a new directional α-mean operation [41]. The experiments have been performed using artificial and real images which demonstrated that it is able to detect edges accurately.

Recently a clustering algorithm named as Neutrosophic Evidential C-Means (NECM) with Dezert–Smarandache Theory (DSmT) is proposed for natural image segmentation [42]. The DSmT combination rule and decision has been utilized to achieve the final result. The NECM method is tested on both data clustering and image segmentation applications. Further, a Neutrosophic Similarity Score (NSS) method and level set algorithm is introduced for breast segmentation in ultrasound images [43]. First, the breast ultrasound is transformed to the NS domain via three membership subsets and then NSS is defined and used to determine the membership degree of the tumor region. Finally, the level set is employed for tumor segmentation in the NSS image. The results have shown that the method can segment the breast tissue in ultrasound images effectively and accurately.

Another neutrosophic domain segmentation method named as Spatial Neutrosophic Distance Regularizer Level Set (SNDRLS) method is presented for automated delineation of nodules in thyroid ultrasound images [44].

3. Experimental results and discussion

3.1. Results of denoising on synthetic images

This section demonstrates the qualitative and quantitative results to evaluate the effectiveness of the neutrosophic domain speckle reduction methods. In experiments, performance of the neutrosophic domain speckle reduction methods NLEE, NKUAN, NNTV and NNRSNR methods are compared with LEE, KUAN, NTV and NRSNR to study the impact of neutrosophic domain in speckle reduction and edge preservation [45]. Several quantitative measures like Signal to Noise ratio (SNR) and Edge Preservation Index (EPI) have been used for the evaluation of aforementioned methods [45, 46].

For quantitative evaluation of despeckling methods, the experiments are conducted on synthetic images, in which image is corrupted by speckle noise using speckle simulation procedure [30]. The performance of speckle reduction methods have been measured on the speckle simulated images at various noise levels ($\sigma = 0.3,0.4, \ldots .0.9$). Table 1 represents SNR values of noisy image, KUAN, LEE, NKUAN and NLEE methods at various noise levels from $\sigma = 0.3$ to 0.9 for synthetic image. From quantitative results, it has been noticed that the neutrosophic domain methods outperformed the spatial domain methods by achieving higher SNR values. The NKUAN outperformed the KUAN filter by gaining higher values of SNR. Similarly, NLEE has also outperformed the LEE filter by achieving higher SNR values.

Table 1

SNR (dB)					
Noise Level	Noisy Image	KUAN	NKUAN	LEE	NLEE
0.3	21.11	22.11	23.42	23.16	23.97
0.4	19.04	20.72	21.41	21.62	22.73
0.5	17.9	18.73	19.39	20.25	21.88
0.6	16.38	17.18	18.86	19.21	20.24
0.7	15.21	15.88	16.31	17.56	18.96
0.8	13.99	14.64	15.98	16.94	17.51
0.9	3.63	5.71	6.04	7.79	8.53

Figure 2 illustrates EPI of different speckle reduction techniques in which neutrosophic domain methods have high edge preservation as compared to spatial domain methods. From graphical representation as shown in Fig. 2, it is observed that NLEE is able to preserve edges better in neutrosophic domain as compared to LEE method. NLEE method has also been found to be performed better than NKUAN in terms of edge preservation. The results have been compared with spatial-domain speckle reduction filters such as LEE and KAUN. Figure 3 illustrates the results of speckle simulated synthetic image. Fig. 3(a) is the original image, and Fig. 3(b) is the image simulated with speckle noise at 0.5 noise level. Figure 3(c) and Fig. 3(d) are the despeckling results of LEE and KUAN filter, respectively. Figure 3(e) and Fig. 3(f) are the results of the proposed methods i.e. Neutrosophic KUAN (NKUAN) filter and Neutrosophic LEE (NLEE) filter.

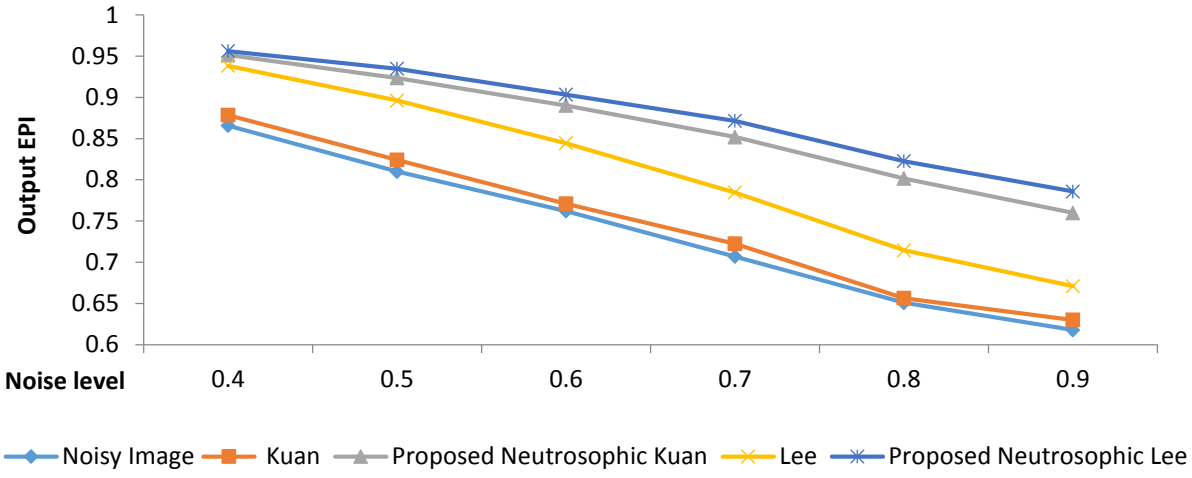

Figure 2: EPI comparison of different techniques on speckle simulated synthetic image.

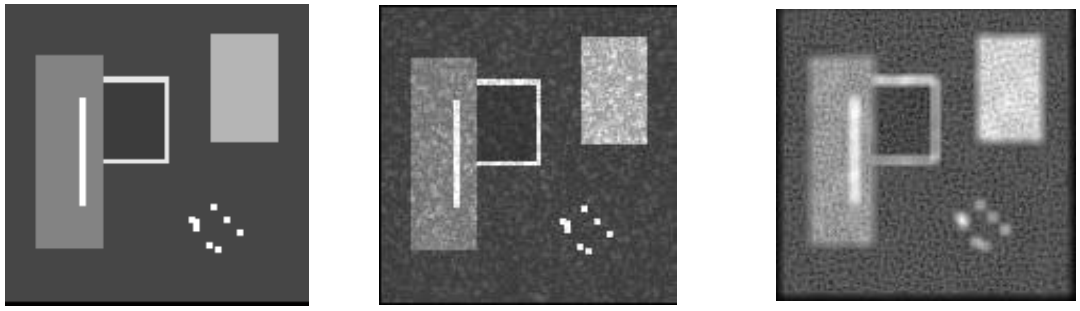

(a) (b) (c)

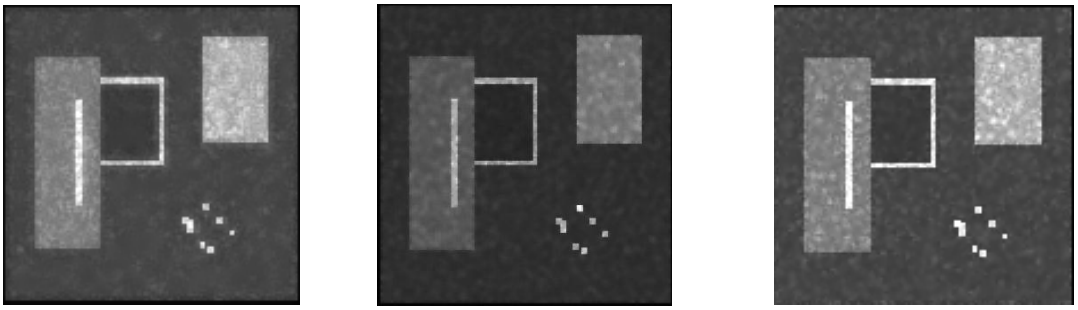

(d) (e) (f)

Figure 3: (a) Original synthetic image (b) Speckle simulated Synthetic image (c) LEE [25] (d) KUAN [26] (e) NKUAN [28] (f) NLEE [28].

Table 2 lists the comparison of different speckle reduction methods such as Nakagami Total Variation (NTV) [29], Neutrosophic Nakagami Total variation (NNTV) [30], Non convex Sparse Regularizer Speckle Noise removal (NRSNR) [50] and Neutrosophic Nonconvex Regularizer Speckle Noise removal (NNRSNR) [27] methods in terms of SNR values at various noise levels from $\sigma = 0.3$ to 0.9. From quantitative results, it has been observed that the neutrosophic domain NNRSNR method outperformed the NRSNR method by achieving higher SNR values. Similarly, neutrosophic domain NNTV outperformed the NTV and other methods by gaining higher SNR value. It is clear from the Table 2 that both neutrosophic domain methods performed better as compared to their counterparts even at high noise levels by achieving maximum SNR values.

Table 2: SNR comparison of different methods at different noise levels (σ = 0.3 to 0.9). SNR is given in dB.

Methods / Variance	Noisy image	NRSNR [50]	NNRSNR [27]	NTV [29]	NNTV [30]
0.3	21.11	22.73	24.22	25.35	26.89
0.4	19.04	22.12	23.03	23.73	24.32
0.5	17.9	22.46	23.73	24.26	25.86
0.6	16.38	21.64	21.98	22.75	23.07
0.7	15.21	18.71	19.66	20.99	21.75
0.8	13.99	17.20	18.37	20.15	20.89
0.9	3.63	6.85	8.75	9.66	10.33
Average	15.32	18.81	19.96	20.98	21.87

Similar type of observations could be made from Fig. 4 with the visual comparison of NRSNR, NTV, NNRSNR and NNTV on speckle simulated phantom image (img1). Figure 4(a) shows an original image and Fig. 4(b) displays the speckle simulated image. Whereas Fig. 4(c) reveals that the NRSNR blurred the image information such as edges. Figure 4(d) illustrates that the neutrosophic domain NNRSNR method performs well in speckle suppression. However, some of the pixels are advertantly suppressed and blurred near the boundaries. Similar type of observation could be made by Fig. 4(e) and Fig. 4(f) that the neutrosophic domain NNTV method has better visual result as compared to its counterpart in terms of speckle reduction and edge preservation.

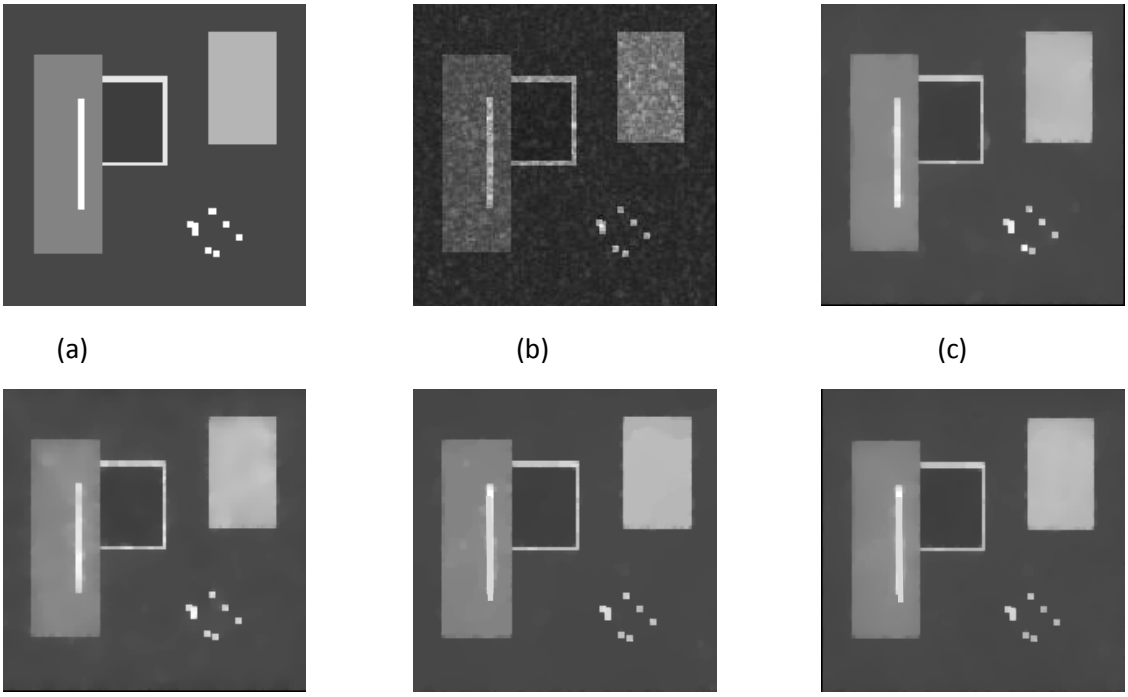

Figure 4: Visual comparison of different methods on speckle-simulated synthetic image (img2) σ = 0.5. (a) Original image (b) Speckle simulated image. Image processed by (c) NRSNR (d) NNRSNR (e) NTV (f) NNTV.

3.2 Results of denoising on real images

Figure 5 shows the results of KUAN, NKUAN, LEE and NLEE methods on medical images. The original image is shown in Fig. 5(a). The NKUAN and NLEE methods have outperformed the KUAN and LEE methods in spatial domain by removing speckle noise as illustrated in Fig. 5.

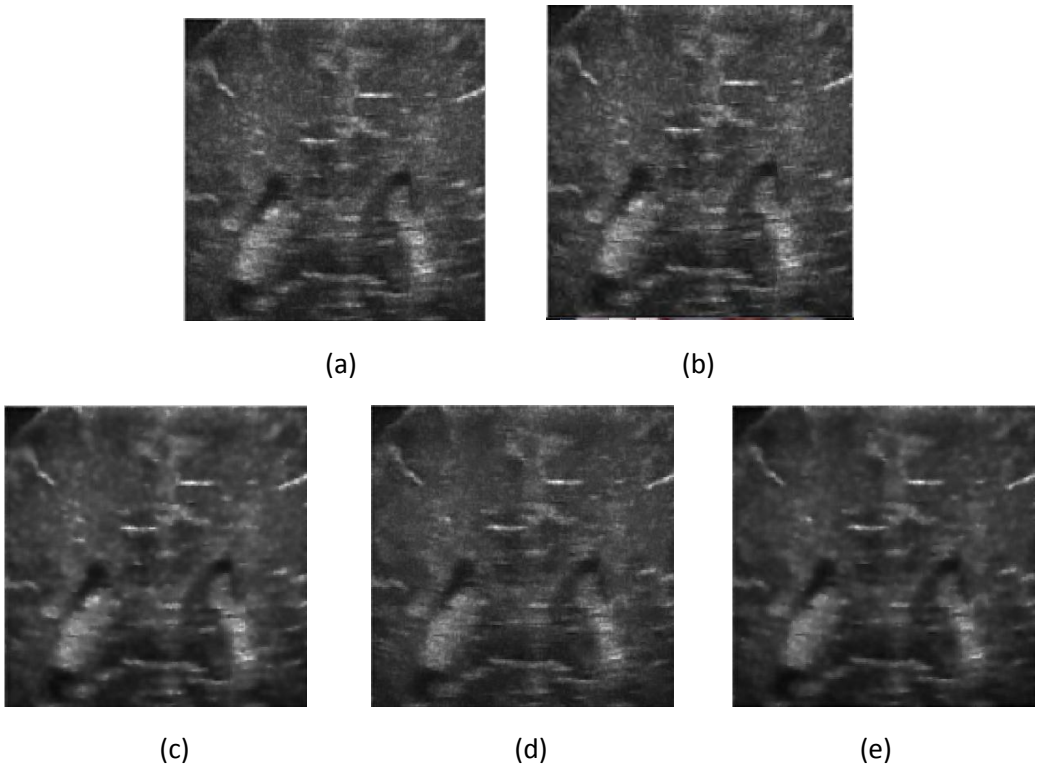

Figure 5: Visual comparison of various methods on (a) test image (b) KUAN (c) NKUAN (d) LEE (e) NLEE.

Figure 6 shows the results of NRSNR, NTV, NNTV and NNRSNR methods on thyroid ultrasound images. The original ultrasound image is given in Fig. 6(a). The NRSNR over-smoothed and blurred the images while speckle removal as illustrated in Fig. 6(b). It caused loss of important details and information of an image. The NNRSNR method has given better results but artifacts can be noticed in Fig. 6(c). The NNTV method effectively removed the speckle noise and preserved the nodule structure as illustrated in Fig. 6(e). Therefore, NNRSNR and NNTV method in neutrosophic domain can lead to efficient nodule detection in the ultrasound image. Small structures which are obscured by speckle noise become visible after processing by neutrosophic domain speckle reduction methods. The NNTV is able to remove speckle pattern, preserve anatomical structures, resolvable details and boundaries. All these results demonstrate the superiority of the neutrosophic domain methods in handling indeterminacy.

These visual outcomes are also evaluated via their line profiles shown in Fig. 7, along the line in the original image. Further, a closer glance in Fig. 7(d) and Fig. 7(f), it is observed that the NNRSNR and NNTV methods surpass the other methods by clearly highlighting the edges of thyroid nodule with the suppression of speckle noise as well as with the preservation of edges and

corners in the thyroid gland ultrasound image. The methods in neutrosophic domain are able to preserve the corners, boundaries and sharp features of the image as shown in Fig. 7. Also the minute subtle details which are hidden by speckle, become noticeable in despeckled image processed by NNTV method.

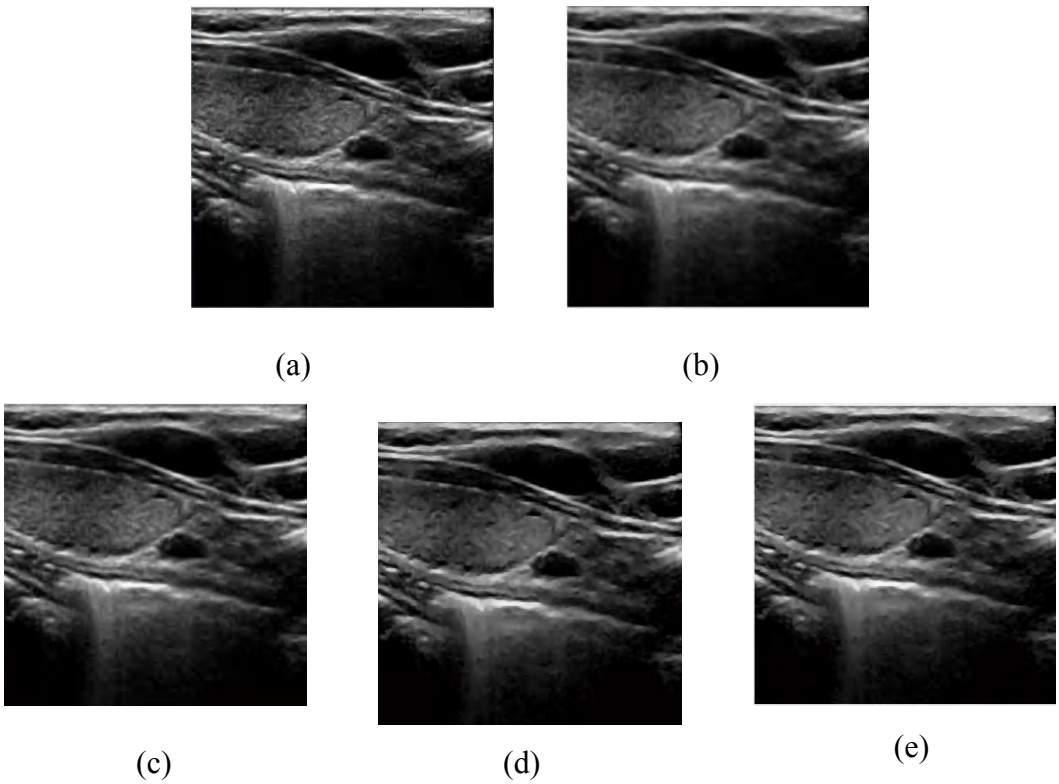

Figure 6: Visual results on the thyroid ultrasound image (img6) (a) Original image. Image processed by (b) NRSNR (c) NNRSNR (d) NTV (e) NNTV.

Further, comparison of NNRSNR and NNTV methods on real ultrasound image is illustrated in Fig. 8. Figure 8(c) shows the despeckled image and its intensity profile is shown in Fig. 8(d) along the highlighted line which revealed that the NNRSNR has lose some important information while removing speckle noise in the filtered image and has changed the contrast of the resultant image. It is observed that the NNTV method using Nakagami distribution can preserved the nodule boundaries better in ultrasound images while the degree of speckle suppression is high as compared to NNRSNR method.

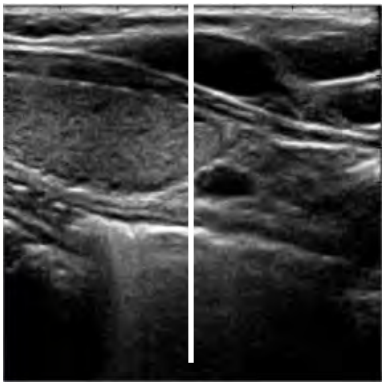

(a)

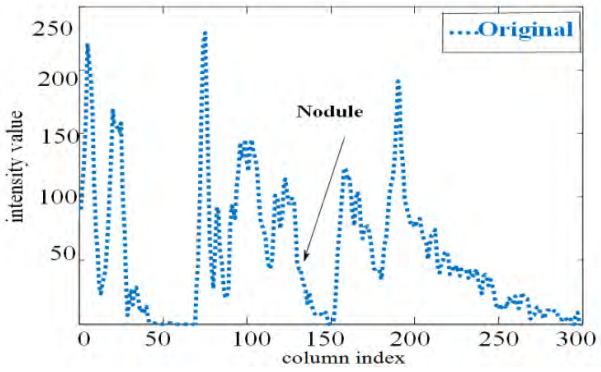

(b)

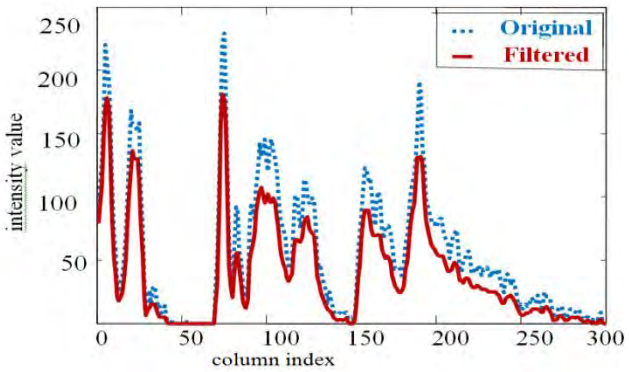

(c)

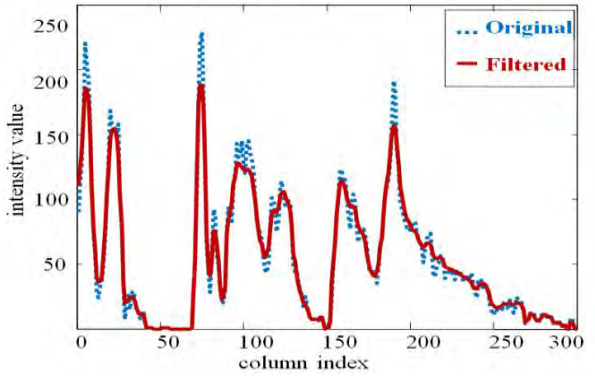

(d)

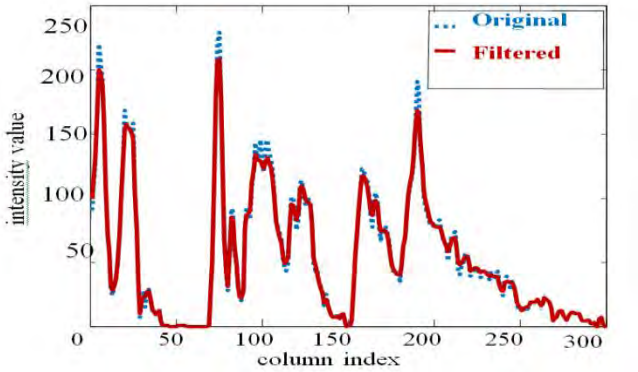

(e)

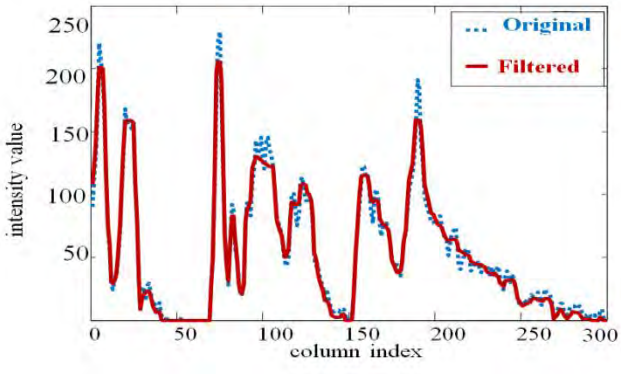

(f)

Figure 7: Line profiles for the thyroid ultrasound image (img6). (a) Original image. (b) Line profile of original image. Line profiles of (c) NRSNR (d) NNRSNR (e) NTV (f) NNTV with original image along the highlighted line.

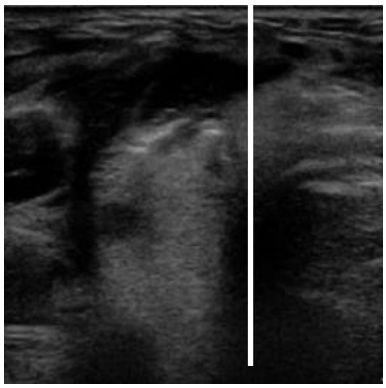

(a)

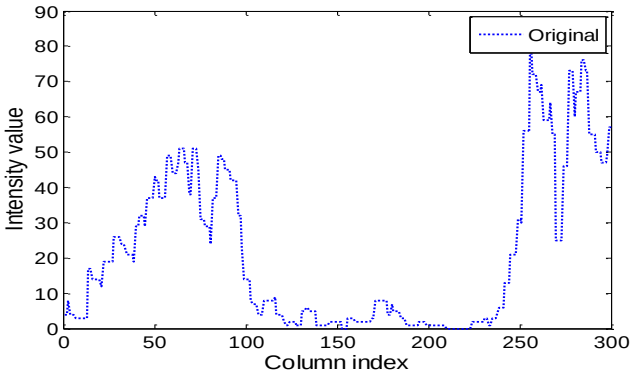

(b)

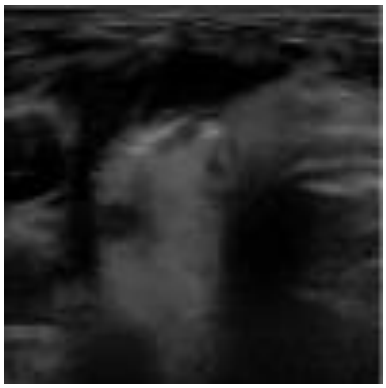

(c)

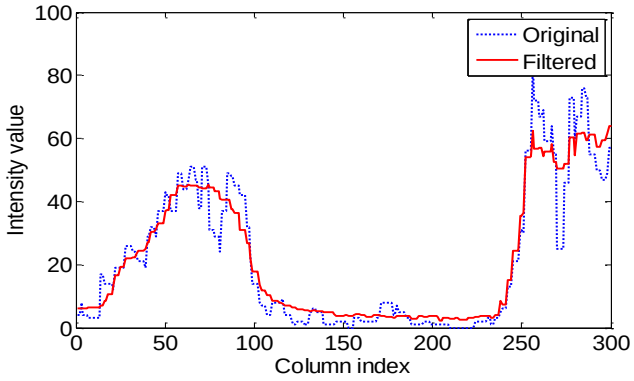

(d)

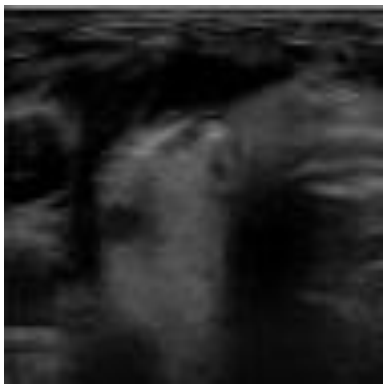

(e)

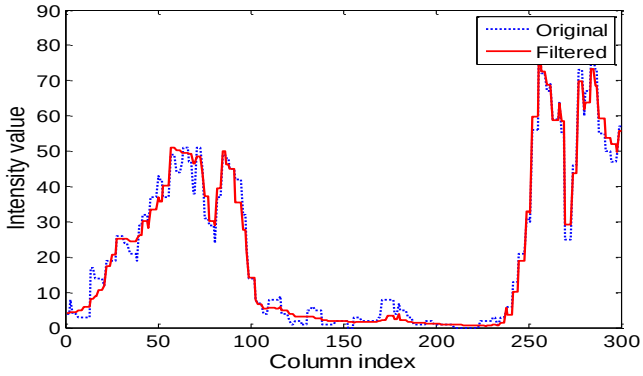

(f)

Figure 8: Denoising results on the thyroid ultrasound image (img8) (a) Original image (b) Line profile of original image (c) Image processed by NNRSNR (d) Line profile of NNRSNR (e) Image processed by NNTV (f) Line profile of NNTV.

1.3. Results of segmentation on real images

Further, the performance of segmentation methods in neutrosophic domain is compared on real ultrasound images [47]. Various performance metrics such as area-based and boundary-based are used to compute how much nodule pixels are correctly covered and to measure the possible disagreement over two curves [48, 49]. Area based metrics which are used in this work are True Positive (TP), False Positive (FP), Dice Coefficient (DC) and Hausdorff Distance (HD).

Table 3 lists the values of all quality metrics. As evident from results, it is observed that SNDRLS outperforms all other neutrosophic domain methods by achieving high values in terms of performance measures. The larger values of area based metrics produced by SNDRLS method assure more similarity between ground truth and the region extracted by automated segmentation method. The SNLM also reveals an improvement in FP value and HD values than other methods as listed in Table 3. The results have shown that more area is achieved by the SNDRLS method in comparison to NCM and NLM.

Table 3: Comparison of segmentation methods

Metrics / Methods	TP (%)	DC (%)	FP (%)	HD (pixels)
NCM [35]	88.5±6.2	78.50±18.4	10.93±10.9	20.1±19.7
NLM [37]	89.0±5.9	88. 00 ±3.9	13.41±13.3	4.3±4.01
SNLM [44]	93.45±2.5	92.8±4.6	4.07±4.8	3.23±0.9
SNDRLS [44]	95.92±3.70	93.88±2.59	7.04±4.21	0.52±0.20

The quantitative results of proposed method are also supplemented with subjective outcomes. Figure 9 shows the comparison of proposed SNDRLS method with all aforementioned methods. Figure 9(a) illustrates the original thyroid ultrasound image and Fig. 9(b) shows the ground truth image. It is observed that the contour segmented by Neutrosophic Watershed (NW) is passed through the weak boundaries as shown in Fig. 9(c).

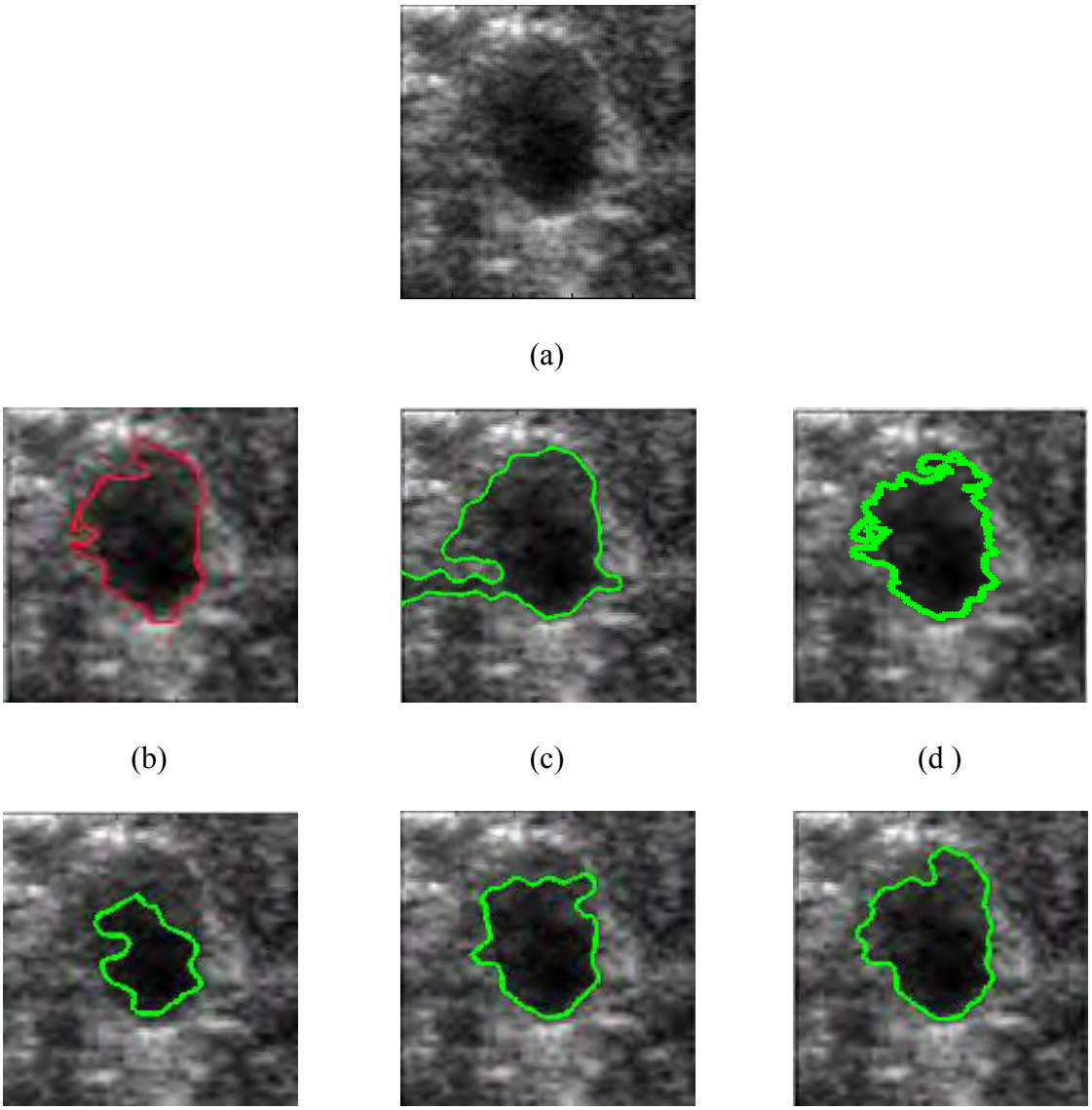

(a) (b) (c) (d) (e) (f) (g)

Figure 9: (a) Ultrasound image (img23) (b) Ground Truth. Segmentation results by (c) Neutrosophic Watershed (NW) [33] (d) NCM [35] (e) NLM [37] (f) SNLM [44] (g) SNDRLS [44].

Neutrosophic C Means (NCM) is affected as it is easily trapped into inappropriate local minima due to similar intensities as illustrated in Fig. 9(d). As evident from Fig. 9(e), NLM method is not able to segment the entire nodule properly. In addition, Fig. 9(f) illustrates the visual outcome of SNLM, which shows that the boundary of segmented nodule is not close to the boundary marked by an expert. It is found that the results of SNDRLS are very close to the manual segmentation as shown in Fig. 9(g). The SNDRLS is able to handle indeterminacy, fuzziness and uncertainty of pixels. From visual results, it has been noticed that the SNDRLS method is effective and accurate

in nodule segmentation using ultrasound images. Figure 10(a) shows the original ultrasound image and Fig. 10(b) illustrates the ground truth image. While from Fig. 10(c), it has been noticed that the nodule is not properly segmented out due to low contrast and weak boundaries. The image segmented by NLM is able to attain delineate nodule regions with non-nodule regions also as shown in Fig. 10(d).

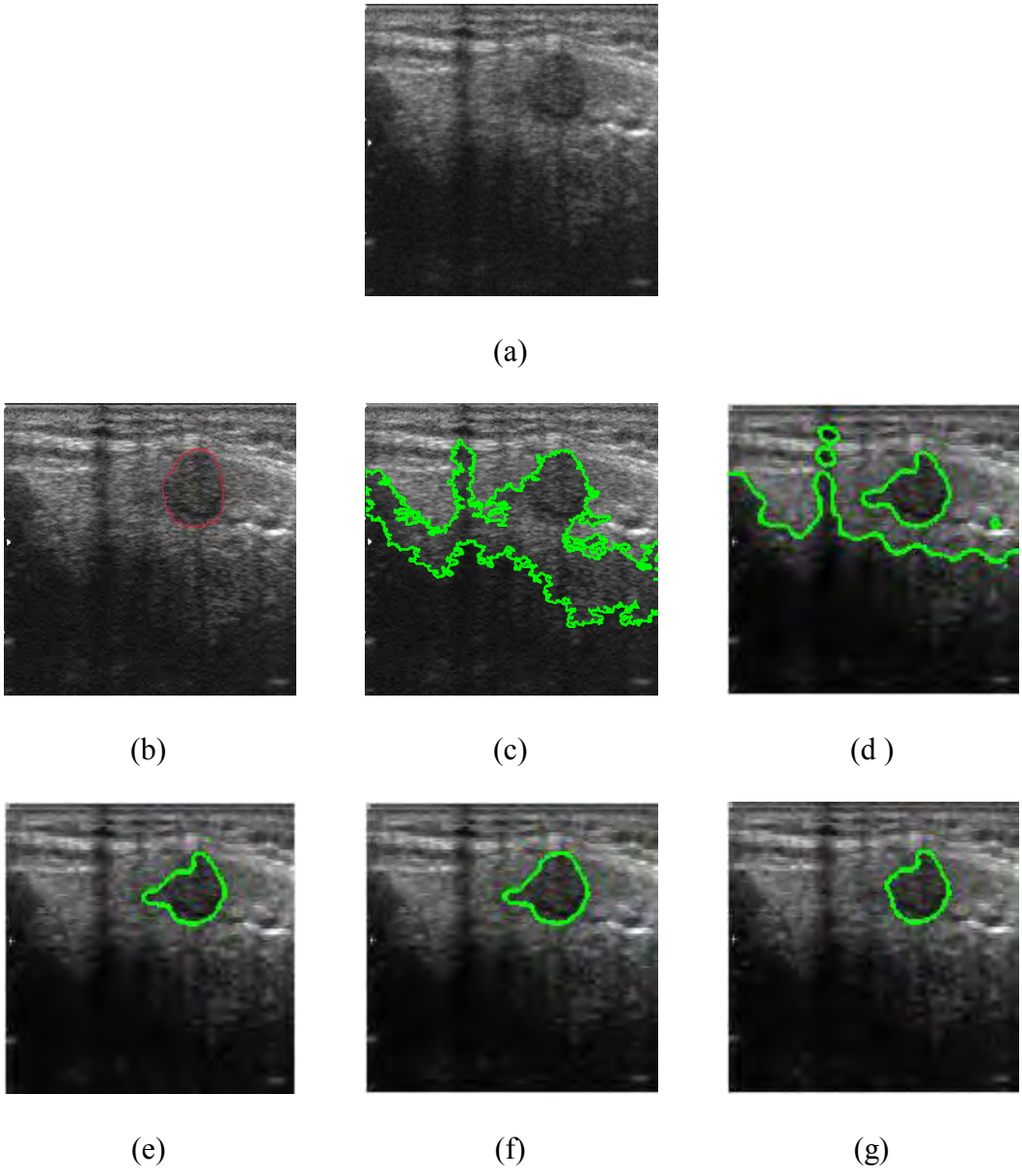

(a)

(b) (c) (d)

(e) (f) (g)

Figure 10: Ultrasound image (img318) (a) Original image (b) Ground Truth. Segmentation results by (c) NW [33] (d) NLM [37] (e) SNLM [44] (f) NCM [35] (g) SNDRLS [44].

The NCM and SNLM are able to segment the nodule in neutrosophic domain but the obtained boundary is not much close to the ground truth boundary as illustrated in Fig. 10(e) and Fig. 10(f). The best segmentation of nodule is achieved by SNDRLS as the attained delineations are very smooth and completely adapted to the thyroid nodule boundaries as shown in Fig. 10(g). Additionally, SNDRLS can prevent leakage through weak edges resulting in accurate extraction of nodule boundaries by handling the intensity in-homogeneity well.

4. Conclusion

Neutrosophic logic gives a powerful tool that can be used to describe the image with uncertain information. This paper provides the usefulness of neutrosophic theory in medical image denoising and segmentation. It is observed that the results using neutrosophic set are much better than the fuzzy/non fuzzy set theory because Neutrosophic set can consider more number of uncertainties by its indeterminacy handling capability. Neutrosophic set gives better result even in low contrasted images with vague region/boundaries. Through the work discussed above shows that neutrosophic based approaches can be utilized for more image processing and pattern recognition applications. It also helps in solving the problems where membership function is not defined accurately due to the lack of personal error.

References

1. Mondal K, Dutta P, Bhattacharyya S. Fuzzy logic based gray image extraction and segmentation. International Journal of Scientific & Engineering Research. 2012;3(4):1-14.
2. Yang Y, Huang S. Image segmentation by fuzzy C-means clustering algorithm with a novel penalty term. Computing and Informatics. 2012;26(1):17-31.
3. Koundal D, Gupta S, Singh S. Applications of neutrosophic and intuitionistic fuzzy set on Image processing. National Conference on Green Technologies: Smart and Efficient Management (GTSEM-2012). 2012.
4. Smarandache F. A Unifying Field in Logics: Neutrosophic Logic. Neutrosophy, Neutrosophic Set, Neutrosophic Probability: Neutrosophic Logic. Neutrosophy, Neutrosophic Set, Neutrosophic Probability. Infinite Study; 2005.
5. Zhang M, Zhang L, Cheng HD. Segmentation of ultrasound breast images based on a neutrosophic method. Optical Engineering. 2010;49(11): 117001-117001.
6. Atanassov KT. Intuitionistic fuzzy sets. Fuzzy sets and Systems. 1986;20(1):87-96.
7. Zhang L, Zhang Y. A novel region merge algorithm based on neutrosophic logic. International Journal of Digital Content Technology and its Applications. 2011;5(7):381-7.
8. Smarandache F. A Geometric Interpretation of the Neutrosophic Set-A Generalization of the Intuitionistic Fuzzy Set. arXiv preprint math/0404520. 2004.
9. Zhang M. *Novel approaches to image segmentation based on neutrosophic logic*. (Doctoral dissertation, Utah State University). 2010.
10. Ju W. *Novel Application of Neutrosophic Logic in Classifiers Evaluated under Region-Based Image Categorization System* (Doctoral dissertation, Utah State University). 2011.
11. Smarandache F. Neutrosophic Logic-Generalization of the Intuitionistic Fuzzy Logic. arXiv preprint math/0303009. 2003.
12. Wang H, Smarandache F, Sunderraman R, Zhang YQ. Interval Neutrosophic Sets and Logic: Theory and Applications in Computing: Theory and Applications in Computing. Infinite Study. 2005(5).
13. Cheng HD, Shan J, Ju W, Guo Y, Zhang L. Automated breast cancer detection and classification using ultrasound images: A survey. Pattern Recognition. 2010;43(1):299-317.
14. Eisa M. A New Approach for Enhancing Image Retrieval using Neutrosophic Sets. International Journal of Computer Applications. 2014;95(8):12-20.

15. Shan J. A fully automatic segmentation method for breast ultrasound images. (Doctoral dissertation, Utah State University). 2011.
16. Guo Y, Cheng HD, Zhang Y. A new neutrosophic approach to image denoising. New Mathematics and Natural Computation. 2009 Nov;5(3):653-62.
17. Guo Y, Şengür A. A novel image segmentation algorithm based on neutrosophic filtering and level set. Neutrosophic Sets and Systems. 2013;1:46-49.
18. Mohan J, Chandra AT, Krishnaveni V, Guo Y. Evaluation of Neutrosophic Set Approach Filtering Technique For Image Denoising. The International Journal of Multimedia & Its Applications (IJMA). 2012;4(4):73-81.
19. Mohan J, Chandra AT, Krishnaveni V, Guo Y. Image Denoising Based on Neutrosophic Wiener Filtering. In Advances in Computing and Information Technology. Springer Berlin Heidelberg. 2013;861-869.
20. Mohan J, Krishnaveni V, Guo Y. Performance analysis of neutrosophic set approach of median filtering for MRI denoising. Int. J Elec. & Commn. Engg & Tech. 2012;3:148-163.
21. Mohan J, Krishnaveni V, Guo Y. MRI denoising using nonlocal neutrosophic set approach of Wiener filtering. Biomedical Signal Processing and Control. 2013;8(6):779-791.
22. Mohan J, Krishnaveni V, Guo Y. A new neutrosophic approach of wiener Filtering for MRI denoising. Measurement Science Review. 2013;13(4):177-186.
23. Qi X, Liu B, Xu J. A Neutrosophic Filter for High-Density Salt and Pepper Noise Based on Pixel-Wise Adaptive Smoothing Parameter. Journal of Visual Communication and Image Representation. 2016;36:1-10.
24. Guo Y, Cheng HD, Zhao W, Zhang Y. A novel image segmentation algorithm based on fuzzy c-means algorithm and neutrosophic set. Proceeding of the 11th Joint Conference on Information Sciences, Atlantis Press. 2008.
25. Lee JS. Digital image enhancement and noise filtering by use of local statistics. Pattern Analysis and Machine Intelligence, IEEE Transactions on. 1980;(2):165-168.
26. Kuan DT, Sawchuk AA, Strand TC, Chavel P. Adaptive restoration of images with speckle. In 26th Annual Technical Symposium of International Society for Optics and Photonics. 1983: 28-38.
27. Koundal D, Gupta S, Singh S. Speckle reduction method for thyroid ultrasound images in neutrosophic domain. IET Image Processing. 2016;10(2):167-75.
28. Koundal D, Gupta S, Singh S. Speckle reduction filter in neutrosophic domain. In Int. Conf. of Biomedical Engineering and Assisted Technologies. 2012:786-790.
29. Koundal D, Gupta S, Singh S. Nakagami-based total variation method for speckle reduction in thyroid ultrasound images. Proceedings of the Institution of Mechanical Engineers, Part H: Journal of Engineering in Medicine. 2016; 230(2):97-110.
30. Koundal D. Automated system for delineation of thyroid nodules in ultrasound images. 2016 (Doctoral dissertation, Panjab University, Chandigarh, India).
31. Cheng HD, Guo Y. A new neutrosophic approach to image thresholding. New Mathematics and Natural Computation. 2008;4(03):291-308.
32. Guo Y, Cheng HD. New neutrosophic approach to image segmentation. Pattern Recognition. 2009;42(5):587-595.
33. Zhang M, Zhang L, Cheng HD. A neutrosophic approach to image segmentation based on watershed method. Signal Processing. 2010;90(5):1510-1517.
34. Guo Y, Sengur A. A novel color image segmentation approach based on neutrosophic set and modified fuzzy c-means. Circuits, Systems, and Signal Processing. 2013;32(4):1699-1723.
35. Guo Y, Sengur A. NCM: Neutrosophic c-means clustering algorithm. Pattern Recognition. 2015;48(8):2710-2724.
36. Sengur A, Guo Y. Color texture image segmentation based on neutrosophic set and wavelet transformation. Computer Vision and Image Understanding. 2011;115(8):1134-1144.
37. Shan J, Cheng HD, Wang Y. A novel segmentation method for breast ultrasound images based on neutrosophic l-means clustering. Medical physics. 2012;39(9):5669-5682.

38. Karabatak E, Guo Y, Sengur A. Modified neutrosophic approach to color image segmentation. Journal of Electronic Imaging. 2013;22(1):013005(1-11).
39. Guo Y, Zhou C, Chan HP, Chughtai A, Wei J, Hadjiiski LM, Kazerooni EA. Automated iterative neutrosophic lung segmentation for image analysis in thoracic computed tomography. Medical physics. 2013;40(8):1-11.
40. Guo Y, Şengür A. A novel image segmentation algorithm based on neutrosophic filtering and level set. Neutrosophic Sets and Systems. 2013;1:46-9.
41. Guo Y, Şengür A. A novel image edge detection algorithm based on neutrosophic set. Computers & Electrical Engineering. 2014;40(8):3-25.
42. Guo Y, Sengur A. NECM: Neutrosophic evidential c-means clustering algorithm. Neural Computing and Applications. 2015;26(3):561-71.
43. Guo Y, Şengür A, Ye J. A novel image thresholding algorithm based on neutrosophic similarity score. Measurement. 2014;58:175-86.
44. Koundal D, Gupta S, Singh S. Automated delineation of thyroid nodules in ultrasound images using spatial neutrosophic clustering and level set. Applied Soft Computing. 2016;40:86-97.
45. Mazzetta J, Caudle D, Wageneck B. Digital camera imaging evaluation. Electro Optical Industries. 2005:8.
46. Chumning H, Huadong G, Changlin W. Edge preservation evaluation of digital speckle filters. IEEE International in Geoscience and Remote Sensing Symposium. IGARSS. 2002; 4, 2471-2473.
47. http://cimlaboratory.com/?lang=en&sec=proyecto&id=31
48. Clinton N, Holt A, Scarborough J, Yan LI, Gong P. Accuracy assessment measures for object-based image segmentation goodness. Photogrammetric Engineering and remote sensing. 2010;76(3):289-99.
49. Arbelaez P, Maire M, Fowlkes C, Malik J. Contour detection and hierarchical image segmentation. IEEE Transactions on Pattern Analysis and Machine Intelligence. 2011;33(5):898-916.
50. Han Y, Feng XC, Baciu G, Wang WW. Nonconvex sparse regularizer based speckle noise removal. Pattern Recognition. 2013;46(3):989-1001.